https://dx.doi.org/10.1103/PhysRevB.104.195138

Topological properties and self-energy effects of elemental Yb

P. M. Sheverdyaeva,[1] F. Offi,[2] S. Gardonio,[3] L. Novinec,[3,*] M. I. Trioni,[4] D. Ceresoli,[4] S. Iacobucci,[5] A. Ruocco,[2] G. Stefani,[5] L. Petaccia,[6] S. Gorovikov,[6,†] E. Cappelluti,[1] P. Moras,[1] G. Bihlmayer,[7,‡] S. Blügel,[7] and C. Carbone[1]

[1]*Istituto di Struttura della Materia-CNR (ISM-CNR), I-34149 Trieste, Italy*
[2]*Dipartimento di Scienze, Università Roma Tre, I-00146 Rome, Italy*
[3]*Materials Research Laboratory, University of Nova Gorica, 5000 Nova Gorica, Slovenia*
[4]*Istituto SCITEC "Giulio Natta", Consiglio Nazionale delle Ricerche, I-20133 Milano, Italy*
[5]*Istituto di Struttura della Materia (ISM-CNR), Area della Ricerca di Roma 2 Tor Vergata, Via Fosso del Cavaliere 100, 00133 Roma, Italy*
[6]*Elettra Sincrotrone Trieste, Strada Statale 14, km 163.5, I-34149 Trieste, Italy*
[7]*Peter Grünberg Institut and Institute for Advanced Simulation, Forschungszentrum Jülich and JARA, 52425, Jülich, Germany*

(Dated: August 23, 2021)

Recent theoretical calculations predict the presence of Dirac nodal lines with π Berry phase and related topological surface states in alkaline-earth elemental surfaces. So far the experimental verification of these properties has been limited to the case of the Be. Here, we demonstrate the existence of similar nodal lines also in hexagonal close-packed Yb, in the limit of zero spin-orbit coupling. These topological properties emerge after taking into account self-energy corrections, which permit to correctly describe the experimental low energy electronic structure of Yb. By angle-resolved photoemission spectroscopy we provide experimental evidence for topological surface states, which are robust in the presence of the large spin-orbit coupling of Yb.

PACS numbers:

INTRODUCTION

Dirac nodal lines (DNLs) are topological features in the band structure which attracted great attention in recent years. In a DNL material the crossing of conduction and valence bands forms a closed path in the momentum space [1]. The topological nature of the DNLs can give rise to several phenomena, such as robust topological surface states (TSSs), a nontrivial Berry phase and the spin Hall effect [1–4]. Among the elemental materials, the alkaline-earth metals Be and Mg, with hexagonal close-packed (*hcp*) structure, and Ca and Sr, with face-centered cubic structure (*fcc*), were predicted to have DNLs with a π Berry phase near the Fermi level in the limit of vanishing spin-orbit coupling (SOC) [2, 5]. The existence of DNLs and TSSs was demonstrated to explain many exotic properties of alkaline-earth metals, such as anomalously high electron-phonon coupling [6], giant Friedel oscillations [7] and a semimetal-semiconductor transition [8, 9]. An experimental verification of the theoretical predictions was limited to the Be(0001) surface, where the projection of the DNL as well as a circular contour, related to a TSS, were experimentally observed by angle-resolved photoemission spectroscopy (ARPES) [5, 10].

Yb is a divalent lanthanide metal with a filled $4f$-shell and close-packed structure at ambient conditions, which shares a number of properties with divalent alkaline-earth metals, including a similar chemical behaviour, semimetal-semiconductor transition under pressure [9, 11] and pressure-induced superconductivity [12]. Close to room temperature Yb was reported to exist in both *fcc* and *hcp* structures [13–16]. Similarly to alkaline-earth metals, *fcc* Yb was predicted to possess a DNL, which becomes gapped due to the large SOC of Yb [2]. The existence of DNL in *hcp* Yb has not yet been addressed. So far, many of the properties of Yb remain not fully understood due to a discrepancy between the experimental and theoretical electronic band structures. Photoemission spectroscopy on close-packed Yb surfaces presents a peaked density of states close to the Fermi level [17–23]. Scanning tunelling spectroscopy on thin Yb films grown on W(110) suggests the existence of an electron pocket at the center of the surface Brillouin zone ($\overline{\Gamma}$) [24, 25]. Instead, band structure calculations do not reproduce this pocket and indicate a semimetallic behaviour for both *hcp* and *fcc* structures [11, 26–31].

With the aim of clarifying the electronic structure of Yb close to the Fermi level we performed a joint DFT and ARPES investigation on Yb(0001) thin films grown on Mo(110). ARPES reveals the existence of an electron pocket at $\overline{\Gamma}$ in *hcp* Yb. We demonstrate that this pocket can be reproduced in DFT by including self-energy corrections via a Hubbard U correction on the empty d orbitals. The same correction induces a similar pocket also in *fcc* Yb. Within this approach we show the formation of two concentric DNL with $\pm\pi$ Berry phase and related TSSs in the electronic structure of *hcp* Yb. We furthermore provide an ARPES evidence for these TSSs. Our revision of the low-energy electronic structure of Yb calls for a reinterpretation of the electronic and transport properties and for the exploration of novel phenomena in this material.

RESULTS AND DISCUSSION

Figure 1(a) reports ARPES data for thin Yb films on Mo(110). We notice the presence of quantum well states (QWSs) with parabolic-like dispersion centered around $\overline{\Gamma}$, whose number increases with the film thickness (1 monolayer (ML) = 3.1 Å[32]). These states arise from the spatial confinement of the electron wave functions within the films and correspond to the discretization of the electron momentum perpendicular to the surface of a bulk Yb band. The bottom edge of this band at $\overline{\Gamma}$ can be easily determined as the position of the deepest QWS for sufficiently thick films (Fig. 1(b)), as discussed in Refs. 33 and 34. In our case the deepest QWS converges to the band edge that can be estimated to be at 130 meV binding energy, thus indicating that bulk-related states form an electron pocket near $\overline{\Gamma}$. The discontinuities that QWSs present at about 0.2-0.3 $Å^{-1}$ derive from the interaction with bulk band edges of Mo(110) [35], as also observed for other systems and comparable film thickness [36]. The origin of the band doubling close to the 0.55 $Å^{-1}$ in the 32 and 42 ML films (white arrows) will be addressed below.

Our experimental data near the Fermi energy can be compared with the results of DFT calculations. In both *fcc* and *hcp* structures the edges of bulk states that project onto $\overline{\Gamma}$ (i.e. states along ΓL for *fcc* and along ΓA for *hcp*) are above the Fermi energy (black curves in Fig. 1(c,d)), in agreement with previous calculations [26, 28–31]. Strain and SOC effects induce minor changes in the band structure at the Fermi energy (see Ref. 28 and Supplemental material Section I and Figures S1-S2). As proposed in an earlier work on Yb [28], one can obtain a good agreement between theory and experiment by tuning the position of the unoccupied *d* bands. Indeed, the experimental band structure of Yb is similar to the ones of *fcc* Ca(111) and *hcp* Mg(0001) [37, 38], which have higher *d* band and an electron pocket located at the L and Γ bulk points, respectively [2, 5]. We applied the Hubbard *U* correction on the *d* orbitals of Yb: Since the conduction band consists mainly of *d* states, the effect of the U_d is similar to the one induced by the self-energy correction, as already demonstrated for other elements of the lanthanide group [39]. Fig. 1(c,d) shows DFT calculations with U_d = 4 eV (red curves), with a *p*-like band crossing the Fermi level in both *fcc* and *hcp* structures, which correctly reproduces the electron pocket observed experimentally. These results are in agreement with the previously demonstrated predominant *p*-character of the Yb states below the Fermi level [22].

Before discussing in detail the electronic structure of Yb, we briefly address the crystallographic structure of our thin films. Yb is known to undergo a $hcp - fcc$ transition close to room temperature with a high degree of hysteresis and sensitivity to the strain and contamination [13–16]. Yb films grown at room temperature and post-annealed at T = 465 K on Mo(110) and W(110) were shown to have a *fcc* structure [17, 32]. On the other hand, the ARPES data here presented shows that the growth at room temperature and without annealing occurs in the *hcp* structure. This is proven by simple symmetry considerations of the bulk *hcp* and *fcc* reciprocal zone and of the way the bulk states are projected on the

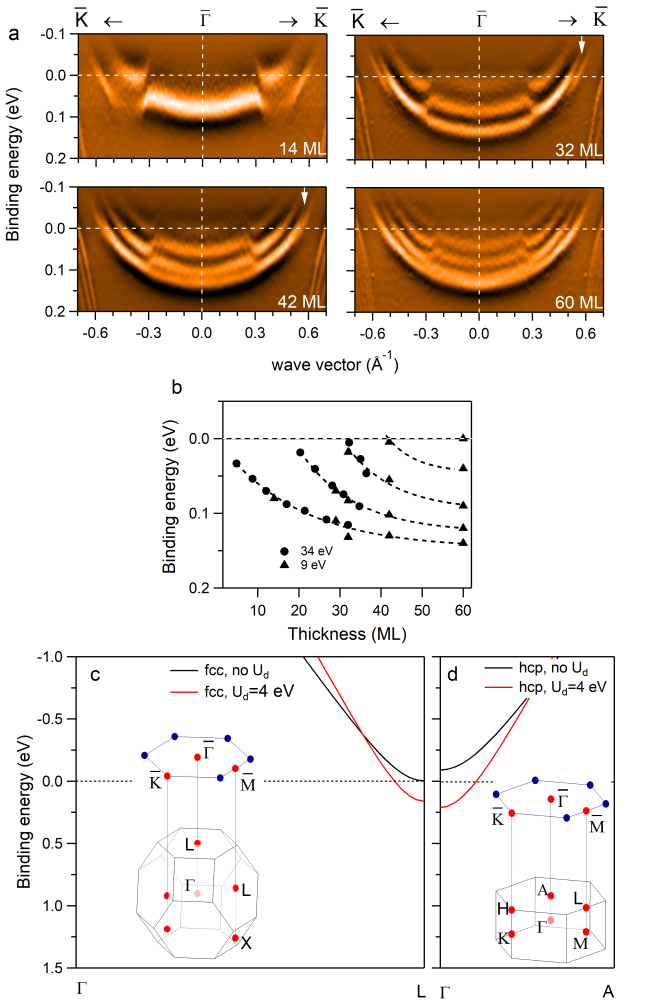

FIG. 1: (a) ARPES maps taken with $h\nu$ = 9 eV at room temperature along $\overline{\mathrm{K}}\,\overline{\Gamma}\,\overline{\mathrm{K}}$ direction and around E_F for different thicknesses as indicated. The images are taken around the $\overline{\Gamma}$ point, normalized to the Fermi function and in a form of second derivative. (b) Energy position versus film thickness of the bands at the $\overline{\Gamma}$ point represented by solid symbols (circles for the experiment obtained at $h\nu$ = 34 eV and triangles for experiments obtained at $h\nu$ = 9 eV); the dashed lines are a guide to the eyes. (c) Theoretical bulk band dispersion without SOC effects along ΓL high symmetry line of *fcc* structure. The inset shows the correspondence of the bulk and surface *fcc* Brilloun zones. (d) Theoretical bulk band dispersion without SOC effects along ΓA high symmetry line of *hcp* structure. The inset shows the correspondence of the bulk and surface *hcp* Brilloun zones.

surface Brillouin zone (Fig. 1(c,d)). In the *fcc* structure the L point is projected on the $\overline{\Gamma}$ and $\overline{\mathrm{M}}$ points of the (111) surface (Fig. 1(c)). Hence, electronic states with the same binding energy must be observed at $\overline{\Gamma}$ and at $\overline{\mathrm{M}}$ (as can also be seen in Supplemental material, section I and Fig. S3). This is in contrast with our ARPES data for all Yb films, in which no states are seen close to the Fermi level at $\overline{\mathrm{M}}$. As an example, Fig. 2(a) shows ARPES spectra for a 29 ML Yb film along the $\overline{\mathrm{K}}\,\overline{\Gamma}\,\overline{\mathrm{M}}\,\overline{\mathrm{K}}$ path. Instead, in the *hcp* structure the $\overline{\Gamma}$ and $\overline{\mathrm{M}}$ points of the (0001) surface are projections of different paths of the bulk Brillouin zone, namely ΓA and ML (Fig. 1(d)), in agreement with the ARPES data.

Figure 2(b,c,d) show DFT slab results for a 24 ML free standing *hcp* Yb film. As expected, without U_d correction there is no electron pocket at $\overline{\Gamma}$ (see Fig. 2(b)). The inclusion of U_d moves the QWSs at $\overline{\Gamma}$ below the Fermi level and they acquire nearly parabolic shapes (Fig. 2(c)), in agreement with ARPES data (Fig. 2(a)). Additionally, a hole pocket emerges between $\overline{\Gamma}$ and $\overline{\mathrm{M}}$. The inclusion of SOC effects results in a splitting of several states with surface character (Fig. 2(d)), without significant energy shifts. A calculated band structure with a different U_d value is shown in Supplemental material, section II and Fig. S4. A similar effect of the U_d correction is expected also for *fcc* thin films. Several surface states marked A, A' and B (Fig. 2(d)) can be identified, while no surface state is observed at $\overline{\Gamma}$ (see also the Supplemental material, section II and Fig. S5). As will be shown below, the A and A' states arise from topological properties of the bulk band structure.

Figure 3(a,b) shows the calculated bulk band structure of *hcp* Yb along KΓMK high symmetry lines in the limit of zero SOC without and with U_d, respectively. We notice that the band structure is strongly modified by the inclusion of U_d, inducing band crossings along ΓM, which otherwise are absent. As a result, there are two band crossings with *s*-*p* band inversion along the ΓK and ΓM directions (black arrows in Fig. 3(b) and red/blue circles in Figs. 3(c,d)) that extend over the Brilloiun zone and give rise to two DNLs. The Berry phase integrated around the loop in k-space enclosing the DNL marked by the red (blue) circle is $-\pi$ ($+\pi$). These DNLs are different from the ones in *hcp* Be and Mg and more similar to that of *fcc* Ca [2, 5]. Indeed, there are two closely lying concentric DNLs. The DNL marked by the red color lies very close to the Fermi energy, resulting in a nearly flat contour, as in Ca(111). The projection of the two DNLs onto the (0001) surface is schematically shown in Fig. 3(e) by red and blue lines. The grey shaded region between them, indicating a range of states where the band inversion occurs and corresponding to a Zak phase = π [2], does not include any time-reversal invariant momenta. Additionally, the SOC opens up a sizeable gap at the Fermi level, as it can be seen in Figs. 3(c,d). Therefore, no DNL can be directly observed [2]. In contrast, for the

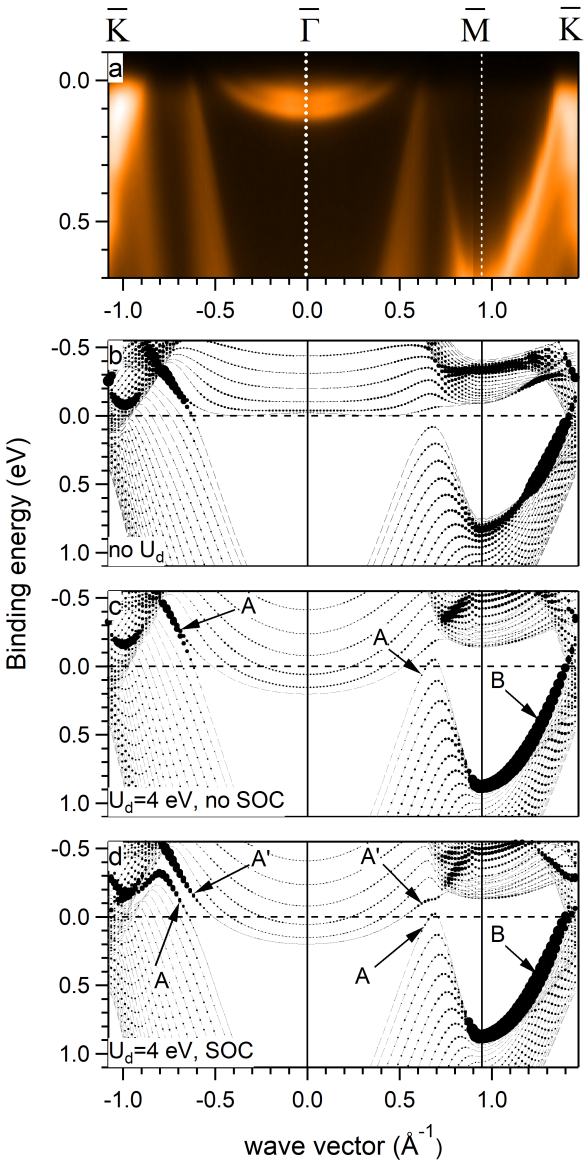

FIG. 2: (a) Photoemission intensity map along the $\overline{\mathrm{K}}\,\overline{\Gamma}\,\overline{\mathrm{M}}\,\overline{\mathrm{K}}$ of a 29 ML Yb film for $h\nu = 34$ eV; (b,c) Calculated surface band structure of 24 ML Yb (0001) film, line thickness is proportional to the s+p+d-character in the top two layers. (b) without U_d, no SOC; (c) with U_d=4 eV, no SOC; (d) with U_d=4 eV, SOC. Black arrows indicate the surface states A, A' and B.

Yb in the *fcc* structure the inclusion of U_d induces almost no change in the topology of the DNL with respect to the band structure calculated without U_d (See supplemental material Section I and figures S1-S2).

In analogy to the Ca(111) surface, we can identify the DNL-related TSSs in Yb(0001). Without SOC we can observe a state A (Fig. 2(c)), which crosses the Fermi level once along $\overline{\Gamma\mathrm{K}}$ and twice along $\overline{\Gamma\mathrm{M}}$ (see also Supplemental material, Section II and Figure S5). Differently from the Ca(111) TSS, without SOC this state is

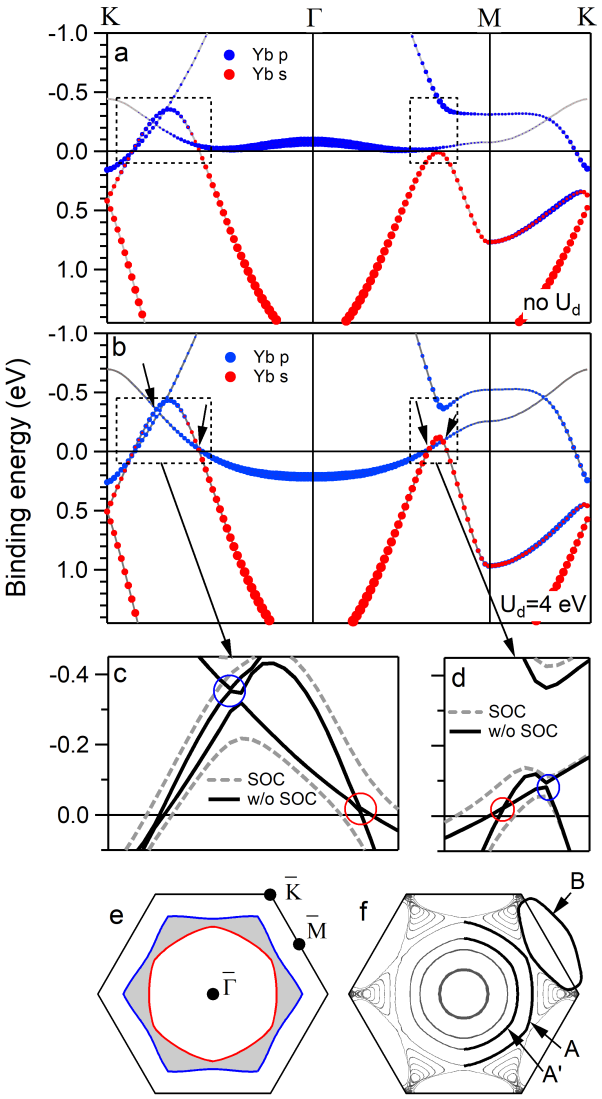

FIG. 3: (a,b) DFT bulk band structure of *hcp* Yb along KΓMK with orbital projections without SOC (a) without U_d (b) with U_d=4 eV. (c,d) zooms on the band crossing without (black solid) and with (grey dashed) SOC included. Red (blue) circles indicate band-crossings with a integral of the Berry curvature around the nodal line corresponding to -π (+π). (e) Surface Brillouin zone with a shaded region indicating the $k_{\|}$ distribution of the π Zak phase. (f) DFT+U_d constant energy cut taken at Fermi level for a 24 ML film with SOC included corresponding to the same slab with surface band structure shown in Fig. 2(d). Thicker lines mark the surface states A, A' and B.

located inside the bulk projected states. With the inclusion of SOC, A splits in two states A and A' (Fig. 2(d)), so along the $\overline{\Gamma K}$ direction the state A falls inside the bulk band gap, while along $\overline{\Gamma M}$ both the states are resonances. Figure 3(f) shows a calculated Fermi surface of

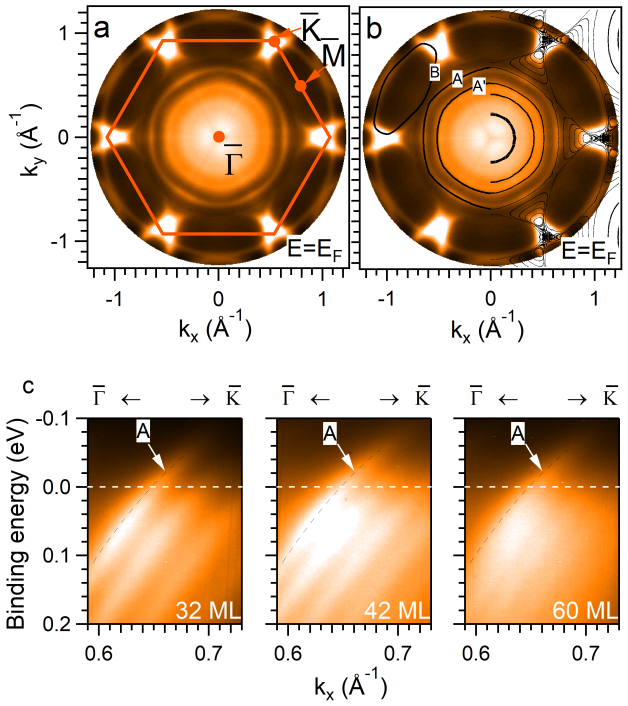

FIG. 4: (a) Constant energy cuts on a 29 ML Yb film with 34 eV photon energy taken at E_F. (b) The same, overlapped with DFT calculated Fermi surface from Fig. 3(f). (c) ARPES maps along $\overline{\Gamma}\,\overline{K}$ direction for different thicknesses as indicated, photon energy 9 eV. The dashed lines are guides to the eye.

24 ML Yb(0001) film, corresponding to the band structure reported in Fig. 2(d). Three concentric contours in the center correspond to the electron pocket. We mark by thicker lines the contours corresponding to A and A' surface states: A' coincides with the outer of the QWSs in the center and A results in a nearly circular shape surrounding A'. Similar TSSs were reported on the surfaces of Ca(111) and Be(0001)[2, 5]. The states A and A' acquire this circular shape only with U_d inclusion, which induces hole and electron pockets along the $\overline{\Gamma M}$ direction. The state B, which is an ordinary surface state, not related to the DNL, forms oval shapes surrounding the $\overline{M}$ points. Similarly to Ca(111) the states A and A' are not topologically protected (Supplemental material, Section III and Figure S6) [2, 5]. A flattening of the bands would lead to disappearing of the DNL and therefore of the states A and A'.

Experimental evidence for all three surface states is provided in Fig. 4(a) showing the experimental Fermi surface. We overlap it with the calculated Fermi surface in the panel (b). We notice a very good agreement between the theory and experiment. The cross-like features close to $\overline{K}$ derive from the state B. The broad intensity in the center is related to the QWSs and the state A'. We can also observe a sharp and intense circular contour whose position matches the state A. We notice that

the intensity of the contour is higher when it approaches the $\overline{\Gamma K}$ direction, where according to the calculations the state A is located inside a gap. Fig. 4(c) shows a zoom on the ARPES data close to the $k_{\|}$ position of contour A for several film thicknesses along $\overline{\Gamma K}$. As one can see this state remains at the same position for different film thicknesses in accord with its surface origin. The state A' can be observed in Fig. 1(a) as a doubling of the QWSs at approximately 0.55 Å^{-1}. The doubling is clear for 32 ML films, becoming smaller in 42 ML and disappearing for thicker films. We can notice the states A and A' also along $\overline{\Gamma M}$ direction, where for relatively thin films there are two states just above the Fermi level which remain at the same $k_{\|}$ position (Supplemental material, section IV and Fig. S7). The state B, in turn, can be clearly seen in Fig. 2(a) as a bright feature along $\overline{MK}$ direction.

As a last point, our study revisits the low-energy electronic structure of Yb and can help to reinterpret the electronic and transport properties of this material, as well as suggests novel ones. In particular, the self-energy correction reveals new topological properties of the poorly explored *hcp* Yb. The two DNLs have π Berry phase, are gapped along all the momentum space due to large SOC and are located very close to the Fermi level. These band structure properties are important for the spin Hall effect: As recently reported, multiple DNLs together with gap opening due to large SOC lead to large spin Hall conductivity [3, 4]. The π Zak phase, in turn, leads to surface polarization charge and can result in substantial deformation of the lattice structure, that needs be explored[2]. Finally, the existence of the electron pocket in the band structure of *fcc* Yb was previously hypothesized in order to explain the resistivity and Hall data and phase transitions in Yb [14, 28]. Also, the recently reported semimetal-semiconductor transition [11], pressure-induced superconductivity [12] and the lifetimes of excited electrons in Yb [30, 31] were analysed on the basis of rather different bulk band structure with no electron pocket at L and should be revisited. In general, our results indicate that in the calculation of Yb compounds, self-energy effects are more important than previously assumed.

CONCLUSIONS

We have studied the electronic structure of *hcp* Yb thin films grown on Mo(110) by ARPES and DFT. ARPES evidences an electron pocket at $\overline{\Gamma}$ that can be reproduced by DFT calculations only by taking into account self-energy corrections on the d states. We furthermore discovered two Dirac nodal lines with a $\pm\pi$ Berry phase near the Fermi level, which emerge when spin–orbit interaction is neglected. The same approach predicts that an electron pocket forms at $\overline{\Gamma}$ also in *fcc* Yb. Dirac nodal line-related topological surface states predicted by theory are experimentally confirmed by ARPES. These unraveled topological properties open a pathway to novel transport properties in this material.

METHODS

The ARPES experiments were performed at the VUV-Photoemission and BaDElPh [40] beamlines at the Elettra synchrotron radiation facility in Trieste, Italy. Photoelectron spectra were recorded at room temperature with a total instrumental energy resolution of 10 meV and an angular resolution of 0.25° at different photon energies ranging from 6 eV up to 40 eV. The Mo(110) surface was cleaned by repeated high temperature flash-annealing cycles in oxygen atmosphere up to 2000 K, until low-energy electron diffraction (LEED) and X-ray photoelectron spectroscopy indicated a clean and ordered surface. Yb was deposited at room temperature by electron-beam evaporation from a Ta crucible using a deposition rate of about 5 Å/min. The base pressure of the experimental station rose 1×10^{-10} mbar to 1×10^{-9} mbar during Yb deposition. A quartz microbalance was used to monitor the thickness of the deposited film. The evaporation rate was cross checked by monitoring the Yb $4f$ core level [41, 42]. The deposition of Yb on Mo(110) at room temperature in the investigated thickness range of $4-60$ ML leads to a well-ordered epitaxial film having a hexagonal (1×1) LEED pattern.

We calculated the electronic structure of the different Yb phases using the full-potential linearized augmented planewave method as implemented in the FLEUR code [43], based on density functional theory with the exchange correlation potential in the generalized gradient approximation [44]. The $5s$ and $5p$ orbitals of Yb were treated as local orbitals and the DFT+U method in the fully localized limit was employed for the $4f$ states with $U_f = 6.0$ eV and $J_f = 0.7$ eV. Where mentioned, also the $5d$ orbitals were treated with the DFT+U method in the fully localized limit using $U_d = 4.0$ eV and $J_d = 0.7$ eV and spin-orbit coupling was included in a self-consistent manner. A product of wavefunction cutoff times muffin-tin radius of 11.2 and optimized lattice parameters of $a_{hex} = 3.852$ Å and c/a = 1.633 with a 8×8×4 k-point set for the *hcp* bulk phase (8×8×8 for *fcc*) were used. The films were set up containing 24 closed-packed layers embedded in vacuum [45] showing negligible relaxations of the surface layers (<0.4%). For the calculation of the Berry curvatures we constructed Wannier functions for the (s,p,d) orbitals and used the WannierTools code [46].

ACKNOWLEDGMENTS

We gratefully acknowledge the computing resources on the supercomputer JURECA at the Jülich Supercomputing Centre (JSC). S.B. acknowledges financial support from the Deutsche Forschungsgemeinschaft through SFB 1238 (Project No. C01). We acknowledge EROFEL-ROADMAP ESFRI of the Italian Ministry of Education, University and research, and the Convenzione Operativa "Tecnologie quantistiche per lo studio di sistemi alla nanoscala rilevanti alla realizzazione di applicazioni sensoristiche biomedicali, magnetiche ed elettroniche" between ISM-CNR and Dipartimento di Scienze of the University "Roma Tre".

* Present address: Elettra Sincrotrone Trieste, Strada Statale 14, km 163.5, I-34149 Trieste, Italy

† Present address: Canadian Light Source Inc., 44 Innovation Boulevard, S7N 2V3 Saskatoon, SK, Canada

‡ Corresponding author: g.bihlmayer@fz-juelich.de

[1] A. A. Burkov, M. D. Hook, and L. Balents, "Topological nodal semimetals," *Phys. Rev. B*, vol. 84, p. 235126, Dec 2011.

[2] M. Hirayama, R. Okugawa, T. Miyake, and S. Murakami, "Topological Dirac nodal lines and surface charges in fcc alkaline earth metals," *Nature Communications*, vol. 8, 2017.

[3] Y. Sun, Y. Zhang, C.-X. Liu, C. Felser, and B. Yan, "Dirac nodal lines and induced spin Hall effect in metallic rutile oxides," *Phys. Rev. B*, vol. 95, p. 235104, Jun 2017.

[4] W. Hou, J. Liu, X. Zuo, J. Xu, X. Zhang, D. Liu, M. Zhao, Z.-G. Zhu, H.-G. Luo, and W. Zhao, "Prediction of crossing nodal-lines and large intrinsic spin Hall conductivity in topological Dirac semimetal Ta3As family," *npj Computational Materials*, vol. 7, no. 1, 2021.

[5] R. Li, H. Ma, X. Cheng, S. Wang, D. Li, Z. Zhang, Y. Li, and X.-Q. Chen, "Dirac Node Lines in Pure Alkali Earth Metals," *Phys. Rev. Lett.*, vol. 117, p. 096401, Aug 2016.

[6] R. Li, J. Li, L. Wang, J. Liu, H. Ma, H.-F. Song, D. Li, Y. Li, and X.-Q. Chen, "Underlying Topological Dirac Nodal Line Mechanism of the Anomalously Large Electron-Phonon Coupling Strength on a Be (0001) Surface," *Phys. Rev. Lett.*, vol. 123, p. 136802, Sep 2019.

[7] P. T. Sprunger, L. Petersen, E. W. Plummer, E. Lægsgaard, and F. Besenbacher, "Giant Friedel Oscillations on the Beryllium(0001) Surface," *Science*, vol. 275, no. 5307, pp. 1764–1767, 1997.

[8] J. W. McCaffrey, D. A. Papaconstantopoulos, and J. R. Anderson, "Band structure and pressure-induced electronic transitions in calcium," *Solid State Communications*, vol. 8, no. 24, pp. 2109–2112, 1970.

[9] D. B. McWhan, T. M. Rice, and P. H. Schmidt, "Metal-Semiconductor Transition in Ytterbium and Strontium at High Pressure," *Phys. Rev.*, vol. 177, pp. 1063–1071, Jan 1969.

[10] I. Vobornik, J. Fujii, M. Mulazzi, G. Panaccione, M. Hochstrasser, and G. Rossi, "Surface electron bands and Fermi surface of Be(0001)," *Phys. Rev. B*, vol. 72, p. 165424, Oct 2005.

[11] C. Enderlein, M. Fontes, E. Baggio-Saitovich, and M. A. Continentino, "Linear-in-temperature resistivity close to a topological metal insulator transition in ultra-multi valley fcc-ytterbium," *Journal of Magnetism and Magnetic Materials*, vol. 398, pp. 270–274, 2016.

[12] J. Song, G. Fabbris, W. Bi, D. Haskel, and J. S. Schilling, "Pressure-Induced Superconductivity in Elemental Ytterbium Metal," *Phys. Rev. Lett.*, vol. 121, p. 037004, Jul 2018.

[13] E. Bucher, P. H. Schmidt, A. Jayaraman, K. Andres, J. P. Maita, K. Nassau, and P. D. Dernier, "New First-Order Phase Transition in High-Purity Ytterbium Metal," *Phys. Rev. B*, vol. 2, pp. 3911–3917, Nov 1970.

[14] J. Alderson and C. Hurd, "Hall effect studies in ytterbium through the f.c.c.-h.c.p. transformation," *Solid State Communications*, vol. 11, no. 9, pp. 1245–1248, 1972.

[15] F. X. Kayser, "Diffraction evidence for the existence of an F.C.C. - H.C.P. transformation in Yb," *physica status solidi (a)*, vol. 8, no. 1, pp. 233–241, 1971.

[16] G. A. Lenkov, A. E. Shitov, A. T. Burkov, and M. P. Volkov, "Magnetoresistance of Polycrystalline Ytterbium at Low Temperatures," *Semiconductors*, vol. 53, no. 13, pp. 1853–1855, 2019.

[17] M. E. Dávila, S. L. Molodtsov, M. C. Asensio, and C. Laubschat, "Determination of the lattice relaxation at the Yb(111) surface using chemical-shift photoelectron diffraction," *Phys. Rev. B*, vol. 62, pp. 1635–1638, Jul 2000.

[18] G. Brodén, S. B. M. Hagström, and C. Norris, "Experimental Evidence of Optical Excitation of $4f$ Electrons in Yb," *Phys. Rev. Lett.*, vol. 24, pp. 1173–1174, May 1970.

[19] G. Brodén, S. B. M. Hagström, and C. Norris, "UV-photoemission study of barium, europium and ytterbium," *Physik der Kondensierten Materie*, vol. 15, pp. 327–345, Feb. 1973.

[20] F. Patthey, J.-M. Imer, W.-D. Schneider, H. Beck, Y. Baer, and B. Delley, "High-resolution photoemission study of the low-energy excitations in 4f-electron systems," *Phys. Rev. B*, vol. 42, pp. 8864–8881, Nov 1990.

[21] F. Offi, S. Iacobucci, L. Petaccia, S. Gorovikov, P. Vilmercati, A. Rizzo, A. Ruocco, A. Goldoni, G. Stefani, and G. Panaccione, "The attenuation length of low energy electrons in Yb," *Journal of Physics Condensed Matter*, vol. 22, no. 30, 2010.

[22] F. Offi, P. Vilmercati, L. Petaccia, S. Gorovikov, A. Ruocco, M. I. Trioni, A. Rizzo, A. Goldoni, G. Stefani, G. Panaccione, and S. Iacobucci, "Revisiting the Yb electronic structure with low-energy photoemission spectroscopy," *Phys. Rev. B*, vol. 85, p. 115108, Mar 2012.

[23] G. Rossi and A. Barski, "Observation of occupied 5d states in f.c.c. Yb metal," *Solid State Communications*, vol. 57, no. 4, pp. 277–281, 1986.

[24] D. Wegner, A. Bauer, and G. Kaindl, "Electronic Structure and Dynamics of Quantum-Well States in Thin Yb Metal Films," *Phys. Rev. Lett.*, vol. 94, p. 126804, Apr 2005.

[25] D. Wegner, A. Bauer, and G. Kaindl, "Influence of morphology on quantum-well states of Yb on W(110)," *Japanese Journal of Applied Physics, Part 1: Regular Papers and Short Notes and Review Papers*, vol. 45, no. 3 B, pp. 1937–1940, 2006.

[26] O. Jepson and O. Anderson, "The electronic structure of

h.c.p. Ytterbium," *Solid State Communications*, vol. 9, no. 20, pp. 1763–1767, 1971.

[27] M. Bodenbach, A. Höhr, C. Laubschat, G. Kaindl, and M. Methfessel, "Surface electronic structure of Tm(0001) and Yb(111)," *Phys. Rev. B*, vol. 50, pp. 14446–14451, Nov 1994.

[28] G. Johansen and A. Mackintosh, "Electronic structure and phase transitions in ytterbium," *Solid State Communications*, vol. 8, no. 2, pp. 121–124, 1970.

[29] Y. Kubo, "Self-consistent relativistic band structures of Sr and Yb under normal and high pressure," *Journal of Physics F: Metal Physics*, vol. 17, no. 2, pp. 383–396, 1987.

[30] A. Marienfeld, M. Cinchetti, M. Bauer, M. Aeschlimann, V. Zhukov, E. Chulkov, and P. Echenique, "Experimental time-resolved photoemission and ab initio GW+T study of lifetimes of excited electrons in ytterbium," *Journal of Physics Condensed Matter*, vol. 19, no. 49, 2007.

[31] V. P. Zhukov, E. V. Chulkov, P. M. Echenique, A. Marienfeld, M. Bauer, and M. Aeschlimann, "Excited electron dynamics in bulk ytterbium: Time-resolved two-photon photoemission and GW + T ab initio calculations," *Phys. Rev. B*, vol. 76, p. 193107, Nov 2007.

[32] M. E. Dávila, S. L. Molodtsov, J. Avila, C. Laubschat, and M. C. Asensio, "Structural characterization using spectroscopic techniques of Yb films grown on W(110) under ultrahigh vacuum conditions," *Journal of Applied Physics*, vol. 93, no. 9, pp. 5075–5079, 2003.

[33] N. J. Speer, M. K. Brinkley, Y. Liu, C. M. Wei, T. Miller, and T.-C. Chiang, "Surface vs. bulk electronic structure of silver determined by photoemission," *EPL (Europhysics Letters)*, vol. 88, p. 67004, dec 2009.

[34] T.-C. Chiang, "Photoemission studies of quantum well states in thin films," *Surface Science Reports*, vol. 39, no. 7, pp. 181–235, 2000.

[35] S. Chernov, K. Medjanik, C. Tusche, D. Kutnyakhov, S. Nepijko, A. Oelsner, J. Braun, J. Minár, S. Borek, H. Ebert, H. Elmers, J. Kirschner, and G. Schönhense, "Anomalous d-like surface resonances on Mo(110) analyzed by time-of-flight momentum microscopy," *Ultramicroscopy*, vol. 159, pp. 453–463, 2015. Special Issue: LEEM-PEEM 9.

[36] P. Moras, D. Topwal, P. M. Sheverdyaeva, L. Ferrari, J. Fujii, G. Bihlmayer, S. Blügel, and C. Carbone, "Influence of the substrate bands on the *sp*-levels topology of Ag films on Ge(111)," *Phys. Rev. B*, vol. 80, p. 205418, Nov 2009.

[37] F. Schiller, M. Heber, V. D. P. Servedio, and C. Laubschat, "Electronic structure of Mg: From monolayers to bulk," *Phys. Rev. B*, vol. 70, p. 125106, Sep 2004.

[38] F. Schiller and C. Laubschat, "Surface states at close-packed surfaces of simple metals," *Phys. Rev. B*, vol. 74, p. 085109, Aug 2006.

[39] P. Larson and W. R. L. Lambrecht, "Electronic structure and magnetism of europium chalcogenides in comparison with gadolinium nitride," *Journal of Physics: Condensed Matter*, vol. 18, pp. 11333–11345, nov 2006.

[40] L. Petaccia, P. Vilmercati, S. Gorovikov, M. Barnaba, A. Bianco, D. Cocco, C. Masciovecchio, and A. Goldoni, "BaD ElPh: A 4m normal-incidence monochromator beamline at Elettra," *Nuclear Inst. and Methods in Physics Research, A*, vol. 606, no. 3, pp. 780–784, 2009.

[41] N. Mårtensson, A. Stenborg, Q. Björneholm, A. Nilsson, and J. N. Andersen, "Quantitative studies of metal-metal adhesion and interface segregation energies using photoelectron spectroscopy," *Phys. Rev. Lett.*, vol. 60, pp. 1731–1734, Apr 1988.

[42] Y. S. Dedkov, D. V. Vyalikh, M. Holder, M. Weser, S. L. Molodtsov, C. Laubschat, Y. Kucherenko, and M. Fonin, "Dispersion of $4f$ impurity states in photoemission spectra of Yb/W(110)," *Phys. Rev. B*, vol. 78, p. 153404, Oct 2008.

[43] for a method description see www.flapw.de.

[44] J. P. Perdew, K. Burke, and M. Ernzerhof, "Generalized Gradient Approximation Made Simple," *Phys. Rev. Lett.*, vol. 77, pp. 3865–3868, Oct 1996.

[45] H. Krakauer, M. Posternak, and A. J. Freeman, "Linearized augmented plane-wave method for the electronic band structure of thin films," *Phys. Rev. B*, vol. 19, pp. 1706–1719, Feb 1979.

[46] Q. Wu, S. Zhang, H.-F. Song, M. Troyer, and A. A. Soluyanov, "WannierTools: An open-source software package for novel topological materials," *Computer Physics Communications*, vol. 224, pp. 405–416, 2018.